RIGA TECHNICAL UNIVERSITY

Armands Rudušs

DEVELOPMENT OF NOVEL STRUCTURAL APPROACHES FOR COST-EFFECTIVE OLED EMITTERS

Summary of the Doctoral Thesis

RTU Press
Riga 2022

RIGA TECHNICAL UNIVERSITY
Faculty of Materials Science and Applied Chemistry
Institute of Applied Chemistry

Armands Rudušs
Doctoral Student of the Study Programme "Chemistry"

DEVELOPMENT OF NOVEL STRUCTURAL APPROACHES FOR COST-EFFECTIVE OLED EMITTERS

Summary of the Doctoral Thesis

Scientific supervisors
Associate Professor Dr. chem.
KASPARS TRASKOVSKIS

Professor Dr. chem.
VALDIS KOKARS

RTU Press
Riga 2022

Rudušs, A. Development of Novel Structural Approaches for Cost-Effective OLED Emitters. Summary of the Doctoral Thesis. Riga: RTU Press, 2022. – 36 p.

Published in accordance with the decision of the RTU Promotion Council "P-01" of 10 October 2022, Minutes No. 04030-9.1/33.

This work has been supported by the European Social Fund within the Project No 8.2.2.0/20/I/008 «*Strengthening of PhD students and academic personnel of Riga Technical University and BA School of Business and Finance in the strategic fields of specialization*» of the Specific Objective 8.2.2 *«To Strengthen Academic Staff of Higher Education Institutions in Strategic Specialization Areas»* of the Operational Programme *«Growth and Employment»*

NATIONAL DEVELOPMENT PLAN 2020

EUROPEAN UNION
European Social Fund

INVESTING IN YOUR FUTURE

Cover photo by Armands Rudušs

https://doi.org/10.7250/9789934228346
ISBN 978-9934-22-834-6 (pdf)

DOCTORAL THESIS PROPOSED TO RIGA TECHNICAL UNIVERSITY FOR THE PROMOTION TO THE SCIENTIFIC DEGREE OF DOCTOR OF SCIENCE

To be granted the scientific degree of Doctor of Science (Ph. D.), the present Doctoral Thesis has been submitted for the defence at the open meeting of RTU Promotion Council on December 15, 2022 at 14.00 at the Faculty of Materials Science and Applied Chemistry of Riga Technical University, 3 Paula Valdena Street, Room 272.

OFFICIAL REVIEWERS

Senior Researcher Dr. chem. Pāvels Arsenjans
Latvian Institute of Organic Synthesis, Latvia

Senior Researcher Dr. phys. Mārtiņš Rutkis
Institute of Solid State Physics, University of Latvia, Latvia

Professor Dr. habil. Juozas Vidas Gražulevičius,
Kaunas University of Technology, Lithuania

DECLARATION OF ACADEMIC INTEGRITY

I hereby declare that the Doctoral Thesis submitted for the review to Riga Technical University for the promotion to the scientific degree of Doctor of Science (Ph. D.) is my own. I confirm that this Doctoral Thesis had not been submitted to any other university for the promotion to a scientific degree.

Armands Rudušs ……..
(*signature*)

Date: .....….....……...…

The Doctoral Thesis has been prepared as a collection of thematically related scientific publications complemented by summaries in both Latvian and English. The Doctoral Thesis includes four scientific publications and two publications in conference proceedings. The publications have been written in English, with the total volume of 215 pages, including supplementary data.

CONTENTS

ABBREVIATIONS

A	acceptor
BPhen	4,7-diphenyl-1,10-phenanthroline
CBP	4,4′-bis(9*H*-carbazol-9-yl)-1,1′-biphenyl
Cbz	carbazole
CMA	carbene-metal-amide
CT	charge transfer
CzSi	9-(4-*tert*-butylphenyl)-3,6-bis(triphenylsilyl)-9*H*-carbazole
D	donor
DCC	dicyclohexylcarbodiimide
DCM	dichloromethane
DFT	density functional theory
Dipp	2,6-diisopropylphenyl group
DMAP	4-dimethylaminopyridine
DMF	dimethylformamide
DMSO	dimethyl sulfoxide
DPEPO	bis[2-(diphenylphosphino)phenyl]ether oxide
DSC	differential scanning calorimetry
HOMO	highest occupied molecular orbital
ISC	intersystem crossing
ITO	indium tin oxide
LCD	liquid crystal display
LE	local excitation
LLCT	ligand-to-ligand charge transfer
LUMO	lowest unoccupied molecular orbital
mCBP	3,3′-di(9*H*-carbazol-9-yl)-1,1′-biphenyl
mCP	1,3-di(9*H*-carbazol-9-yl)benzene
Me	methyl group
MLCT	metal-to-ligand charge transfer
NHC	*N*-heterocyclic carbenes
OLED	organic light-emitting diode
OXD-7	1,3-bis[2-(4-*tert*-butylphenyl)-1,3,4-oxadiazo-5-yl]benzene
PEDOT:PSS	poly(3,4-ethylenedioxythiophene) polystyrene sulfonate
Ph	phenyl group
PL	photoluminescence
PolyTPD	poly(4-butylphenyldiphenylamine)
PMMA	poly(methyl methacrylate)
ppy	2-phenylpyridine
PVK	polyvinylcarbazole
RISC	reverse intersystem crossing
RT	room temperature

S	singlet state
SOC	spin-orbital coupling
T	triplet state
TADF	thermally activated delayed fluorescence
TAPC	1,1-bis[(di-4-tolylamino)phenyl]cyclohexane
TCTA	tris(4-carbazoyl-9-ylphenyl)amine
TD-DFT	time-dependent density functional theory
THF	tetrahydrofuran
TmPyPB	1,3,5-tris(3-pyridyl-3-phenyl)benzene
TPBi	1,3,5-tris(1-phenyl-1*H*-benzimidazol-2-yl)benzene
UV	ultraviolet light
Vis	visible light

GENERAL OVERVIEW OF THE THESIS

Introduction

Organic light emitting diode (OLED) is a device that can be used for display and lighting applications. OLED technology provides an opportunity to develop displays that surpass the widely used liquid crystal display (LCD) technology both in performance and aesthetic aspects.[1] The ability to produce thin, flexible, large-area OLED panels opens up a new perspective for the design of decorative lighting elements.[2] Although OLED displays are widely applied in smartphones, such devices as larger area TVs, computer screens and lighting appliances are not available to a wider consumer range due to the high production cost. Potential directions for cost reduction mentioned in literature include an optimization of the OLED manufacturing process and the usage of low-cost materials.[3]

The deposition of the thin device structure-forming layers is the most important process in OLED manufacturing. Currently, the most widely used approach to the production of thin films is vacuum deposition technology. By this method the applicable material passes from solid state to gas phase under the influence of a vacuum and a heat source. Molecules in the gas phase move to the substrate and slowly condense to form a thin film.[4] The requirement for high vacuum, high evaporation temperature of some materials, the loss of material in the vacuum chamber and the technical difficulties associated with the production of large surface area thin layers together increase the cost of the vacuum deposition process.[5] Therefore, more cost efficient methods are required. One of the alternative approaches is the preparation of thin films from solutions, using methods such as spin coating and printing. However, most of the organic emitters used for vacuum deposition are not suitable for solution processing. The main reasons for that are the insufficient solubility of numerous materials as well as the ability of materials to form a homogeneous amorphous phase with high morphological and thermal stability.[6]

The opportunities for modification of the widely used phosphorescent iridium(III) complex OLED emitters in order to obtain solution-processable materials were explored in the first part of the Doctoral Thesis. Iridium(III) complexes were functionalized with trityl (-CPh_3) groups, which leads to an increase of the solubility of the compounds in organic solvents and to improvement of the optical quality and morphological stability of thin amorphous films produced by solution methods. The characterization of photophysical properties of the obtained complexes and assessment of their performance parameters in solution-processed OLEDs were carried in this part of the Thesis.

The costs of OLEDs are increased not only by the complicated manufacturing process. The cost of the used materials (the emitters in particular) should also be considered. Currently, the most important class of emitters with practical application in commercialized OLEDs are phosphorescent iridium(III) complexes.[7] The high cost of rare transition metals and the potential environmental risks encourage replacement of phosphorescent materials with alternatives such as thermally activated delayed fluorescence (TADF) emitters.[8]

In the second part of the Thesis, carbene-metal-amide (CMA) type TADF emitters were synthesized with copper as the complex-forming element. The characterization of the structure

and photophysical properties of the obtained compounds was carried out and the luminescence mechanism was investigated. The practical application of 1,3-thiazol-2-ylidene carbene fragment-based CMA derivatives in efficient white light emitting OLEDs has been demonstrated.

Aims and Objectives

The aim of the Doctoral Thesis is the synthesis of low-molecular weight organic emitters that would lead to reduced production costs of OLED devices. The following objectives are defined for the implementation of the aim of the Doctoral Thesis:

1. Synthesis of phosphorescent iridium(III) organometallic complexes functionalized with trityl groups. Characterization of the photophysical and morphological properties of the obtained compounds in thin amorphous films.
2. Evaluation of the trityl-functionalized iridium(III) complexes for the preparation of high-efficiency OLEDs.
3. Synthesis of luminescent carbene-metal-amide (CMA) type copper(I) organometallic complexes. Structural characterization of the obtained compounds and study of emitter TADF properties.
4. Evaluation of the newly obtained CMA derivatives for the preparation of high-efficiency OLEDs.

Scientific Novelty and Main Results

In the first part of the Doctoral Thesis, two series of trityl-functionalized heteroleptic 2-arylbenzo[d]thiazole ligand-containing and homoleptic 2-phenylpyridine ligand-containing phosphorescent iridium(III) complexes were synthesized. The photophysical and morphological properties of the obtained compounds in thin amorphous films enable the use of the trityl-functionalized iridium complexes for the preparation of solution-processed OLEDs. However, a systematic study of the effect of trityl groups on OLED performance shows that trityl groups negatively affect the charge carrier transport within the emitting layer, which reduces the emission efficiency of OLEDs. Although the obtained data show the limited application of trityl groups as efficient OLED emitters, the results give an insight into the prerequisites that should be taken into account regarding the molecular design of solution-processable iridium(III) complexes.

Two series of novel CMA type TADF emitters were synthesized within the second part of the Doctoral Thesis. In the first series of CMA emitters, imidazole type NHC derivatives with phenylsulfonyl acceptor groups added to the peripheral steric groups are used as carbene fragments. In the second series, 1,3-thiazol-2-ylidene type NHC derivatives serve as the carbene fragment. A novel TADF mechanism of CMA type emitters was observed for phenylsulfonyl-functionalized complexes. The influence of steric effects on the luminescence properties of the compounds was investigated for 1,3-thiazol-2-ylidene derivatives. The potential application of

1,3-thiazol-2-ylidene CMA derivatives in the development of high-efficiency OLED devices was demonstrated.

Structure and Volume of the Thesis

The Doctoral Thesis has been prepared as a collection of thematically related scientific publications dedicated to the synthesis of luminescent trityl-functionalized Ir(III) and CMA type Cu(I) metalorganic complexes, characterization of the photophysical properties and the assessment of the obtained emitters for the development of low-cost OLEDs.

Publications and Approbation of the Thesis

Results of the Thesis have been reported in four scientific publications and two publications in conference proceedings. The results have been presented in seven reports at five conferences.

Scientific publications:

1. **Ruduss, A.**; Turovska, B.; Belyakov, S.; Stucere, K. A.; Vembris, A.; Baryshnikov, G.; Ågren, H.; Lu, J.; Lin, W.; Chang, C.; Traskovskis, K. Thiazoline Carbene–Cu(I)–Amide Complexes: Efficient White Electroluminescence from Combined Monomer and Excimer Emission. *ACS Appl. Mater. Interfaces.* **2022**, *14* (13), 15478–15493. doi: 10.1021/acsami.2c00847. Impact factor of the journal (2021): 10.383.
2. **Ruduss, A.**; Turovska, B.; Belyakov, S.; Stucere, K. A.; Vembris, A.; Traskovskis, K. Carbene–Metal Complexes as Molecular Scaffolds for Construction of Through-Space Thermally Activated Delayed Fluorescence Emitters. *Inorg. Chem.* **2022**, *61* (4), 2174–2185. doi: 10.1021/acs.inorgchem.1c03371. Impact factor of the journal (2021): 5.436.
3. **Ruduss, A.**; Kokars, V.; Tetervenoka, N.; Vembris, A.; Traskovskis, K. Effects of Steric Encumbrance of Iridium(iii) Complex Core on Performance of Solution-Processed Organic Light Emitting Diodes. *RSC Adv.* **2020**, *10* (46), 27552–27559. doi: 10.1039/D0RA04652C. Impact factor of the journal (2021): 4.036.
4. Traskovskis, K.; **Ruduss, A.**; Kokars, V.; Mihailovs, I.; Lesina, N.; Vembris, A. Thiphenylmethane Based Structural Fragments as Building Blocks Towards Solution-Processable Heteroleptic Iridium(iii) Complexes for OLED Use. *New J. Chem.* **2019**, *43* (1), 37–47. doi: 10.1039/C8NJ04484H. Impact factor of the journal (2021): 3.925.

Publications in conference proceedings:

1. Jece, A.; **Ruduss, A.**; Štucere, K. A.; Vembris, A.; Traskovskis, K. TADF Active Carbene-Metal-Amide Complexes Exhibiting Through-Space Charge Transfer: An Impact of Metal Atom. *Organic Electronics and Photonics: Fundamentals and Devices III.* **2022**, 1214909. doi: 10.1117/12.2621156
2. **Ruduss, A.**; Sisojevs, Ž.; Vembris, A.; Štucere, K. A.; Traskovskis, K. Symmetrical versus Asymmetrical Molecular Configuration in Metal-Assisted-Through-Space Charge Transfer TADF Emitters. *Organic Electronics and Photonics: Fundamentals and Devices III*. **2022**, 1214908. doi: 10.1117/12.2620983

Results of the Thesis have been presented at the following conferences:

1. **Ruduss, A.;** Sisojevs, Z.; Vembris, A.; Stucere, K.; Traskovskis, K. Symmetrical Versus Asymmetrical Molecular Configuration in Metal Assisted-Through-Space Charge Transfer TADF Emitters. *SPIE Photonics Europe, Conference 12149, Organic Electronics and Photonics: Fundamentals and Devices III*, Strasbourg, France, April 4–6, **2022**.
2. Jece, A.; **Ruduss, A.;** Vembris, A.; Stucere, K.; Traskovskis, K. TADF active carbene-metal-amide complexes exhibiting through-space charge transfer: an impact of metal atom. *SPIE Photonics Europe, Conference 12149, Organic Electronics and Photonics: Fundamentals and Devices III*, Strasbourg, France, April 4–6, **2022**.
3. **Ruduss, A.**; Sisojevs, Z.; Jece, A. Thiazoline Carbene-Cu(I)-Carbazolide Complexes as Luminescent TADF Materials. *80th International Scientific Conference of the University of Latvia 2022. Chemistry Section*, Riga, Latvia, February 11, **2022**.
4. **Ruduss, A.**; Jece, A.; Balodis, K.; Traskovskis, K. The Use of Thiazoline-Based Carbenes for a Development of Metalorganic Thermally Activated Delayed Fluorescence Emitters. *Riga Technical University 62nd International Scientific Conference "Materials Science and Applied Chemistry"*, Riga, Latvia, October 22, **2021**.
5. Sisojevs, Z.; **Ruduss, A.**; Balodis, K.; Traskovskis, K. Synthesis and photophysical properties of metal-amide complexes of *N*-heterocyclic carbenes containing peripheral acceptor groups. *Riga Technical University 62nd International Scientific Conference "Materials Science and Applied Chemistry"*, Riga, Latvia, October 22, **2021**.
6. **Ruduss, A.**; Traskovskis, K.; Kokars, V. Photophysical Properties of 9,9'-Bis-Methoxypenyl Substituted 3,3'-Bicarbazoles. *13th International Conference on Optical Probes of Organic and Hybrid Optoelectronic Materials and Applications 2019*, Vilnius, Lithuania, July 7–13, **2019**.
7. **Ruduss, A.**; Traskovskis, K.; Otikova, E.; Vembris, A.; Grzibovskis, R.; Kokars, V. 3,3'-Bicarbazole Structural Derivatives as Charge Transporting Materials for Use in OLED Devices. *SPIE Photonics Europe, Conference 10687, Organic Electronics and Photonics: Fundamentals and Devices III*, Strasbourg, France, April 24–26, **2018**.

MAIN RESULTS OF THE THESIS

1. OLED Structure and Basic Principles of Operation

In organic light-emitting diode (OLED) light emission is realized from organic electroluminescent material in the presence of electric current.[9] A simplified model of OLED structure is given in Fig. 1.1.[10] A typical OLED device consists of several thin layers, which are stacked upon one another using glass or other transparent material as a substrate. The thin layers can be deposited using vacuum or solution methods. The utilized materials have to be compatible with the technique used in the deposition of thin layers. Materials must exhibit chemical, photochemical and morphological stability to prevent degradation during the operation of the device.[11]

An external source of electrical current is required for the operation of the device. By applying an electrical voltage, holes (positive charge carriers) and electrons (negative charge carriers) move from the anode and cathode to the emitting layer, respectively. Charge carrier injection layers (not depicted in Fig. 1.1), charge carrier transport layers, and charge carrier blocking layers could be inserted between electrodes and emitting layer to ensure low injection barrier and to provide balanced and effective charge carrier transport.[12] When holes and electrons recombine within an organic molecule in the emissive layer, it is excited. The return of the excited molecules to the ground state with the emission of light is called electroluminescence. The emitter is doped in a special charge carrying host matrix in low concentration. The blend of this type is called guest-host system. The emitter molecules are spatially separated from each other by mixing into the host matrix, therefore reducing intermolecular interactions and quenching of excited states.[13]

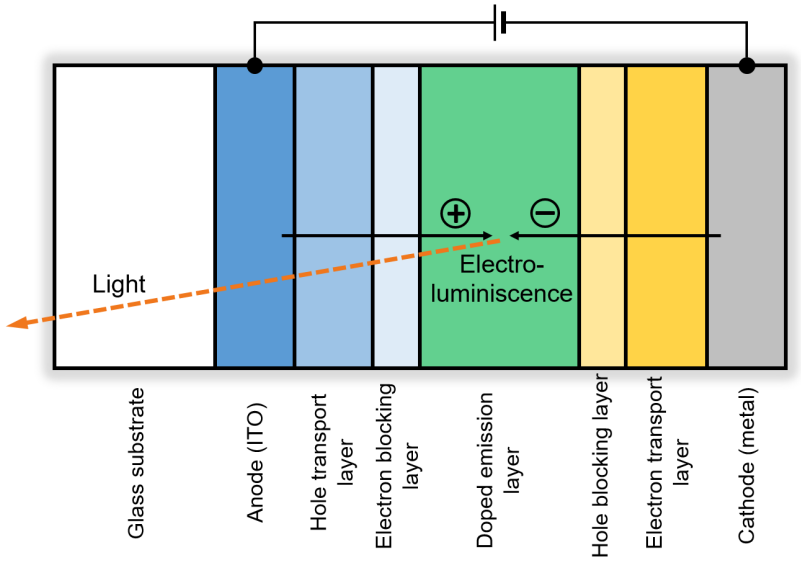

Fig. 1.1. Principal structure of OLED.

Closely bound electron and hole pairs called excitons are formed as a result of the charge carrier recombination. Further exciton relaxation from excited state to ground state can lead to the emission of photon. Therefore, efficient exciton energy transfer to the emitter molecules is essential for ensuring electroluminescence. Two types of excitons (singlet (S) and triplet (T)) are formed during the charge carrier recombination process (Fig. 1.2). Spin statistics determine that the ratio of the produced singlet and triplet excitons is 1:3.[14]

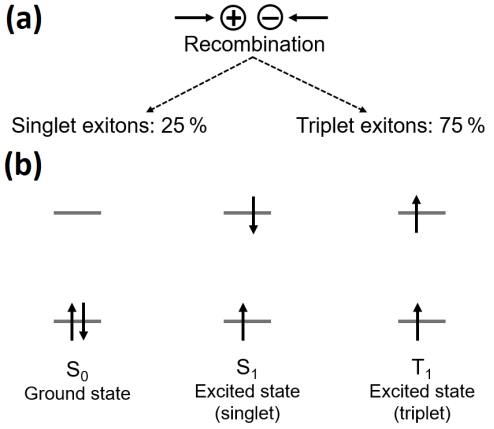

Fig. 1.2. (a) Singlet and triplet exciton formation ratio. (b) Electron spin configuration in ground state S_0 and S_1, T_1 excited states.

A quantitative measure – the luminescence quantum yield (Φ) – is used for the characterization of the emission efficiency of luminescent materials.[15] The quantum yield is defined as the proportion of excited states that emit a photon as a result of radiative relaxation:

$$\Phi = \frac{k_r}{k_r + k_{nr}}, \quad (1.1)$$

where: Φ – quantum yield;
k_r – radiative rate constant;
k_{nr} – non-radiative rate constant.

In practical measurements photoluminescence quantum yield (Φ_{PL}) of materials is determined relatively easily.[15] Photoluminescence quantum yield is measured as the ratio of the photons emitted by the material and the photons absorbed by the material:

$$\Phi_{PL} = \frac{N_{em}}{N_{abs}}, \quad (1.2)$$

where: Φ_{PL} – photoluminescence quantum yield;
N_{em} – the number of photons emitted;
N_{abs} – the number of photons absorbed.

It is necessary to determine photoluminescence quantum yield and photoluminescence lifetime for the calculation of the radiative rate constant[16]:

$$k_r = \frac{\Phi_{PL}}{\tau_{PL}}, \quad (1.3)$$

where τ_{PL} is photoluminescence lifetime.

In the case of fluorescent emitters, only singlet excitons (S_1) are able to relax to the ground state through a photon emission (Fig. 1.3 (a)). The relaxation of the triplet excited state (T_1) to the ground state (S_0) is a spin-forbidden transition and therefore this process (phosphorescence) is characterized with a very long lifetime. Consequently, the emission from the T_1 state is almost completely suppressed by various non-radiative relaxation processes. For this reason, fluorescent OLEDs have a maximum theoretical internal quantum efficiency of 25 %.[17]

The replacement of fluorescent emitters with phosphorescent analogues is considered as one of the methods for increasing the internal quantum efficiency from 25 % to 100 % (Fig. 1.3 (b)). Phosphorescent materials are usually organometallic complexes of heavy transition metals (Ir, Pt, Os, Ru, etc.). In this case heavy metal atoms provide an efficient spin-orbit coupling (SOC). SOC is a process that promotes spin inversion, thereby facilitating intersystem crossing (ISC) as well as phosphorescent relaxation of the T_1 state.[18]

Emitters with thermally activated delayed fluorescence (TADF) properties could be used as an alternative to the phosphorescent materials containing heavy transition metals (Fig. 1.3 (c)). In TADF materials the energy difference between the S_1 and T_1 (ΔE_{ST}) states is lower than 0.1 eV. In this way, reverse intersystem crossing (RISC) is promoted. Thus, the non-radiative triplet states are upconverted into radiative singlets, from which the so-called delayed fluorescence is possible. Both the phosphorescence and TADF mechanisms fully utilize the singlet and triplet excitons in radiative processes, thus achieving the maximum theoretically possible internal quantum efficiency (100 %).[19]

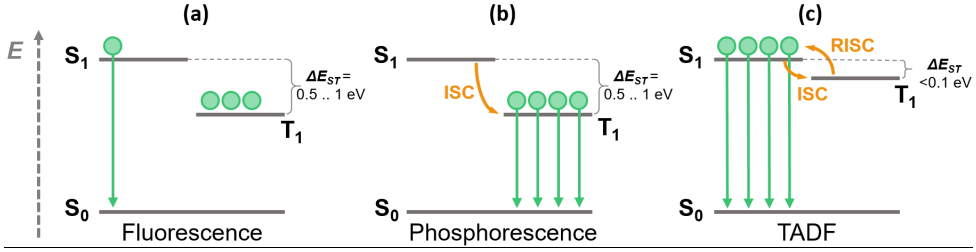

Fig. 1.3. Schematic representation of fluorescence, phosphorescence and TADF mechanisms.

2. Synthesis and Phosphorescence of the Trityl-Functionalized Ir(III) Complexes

The energy-intensive vacuum deposition of the active layer is considered as one of the main problems that leads to significant increases in the OLED manufacturing cost. The vacuum deposition of the OLED emitting layer is especially complicated due to the need to deposit the matrix material together with the emitter (guest-host system). Spin coating from concentrated solutions is as an alternative approach to the deposition of thin films.[20] In order for the material to be suitable for spin coating, not only it must be soluble in volatile organic solvents but also form a stable amorphous phase with a high glass transition temperature and good optical quality. In our previous studies we discovered that the functionalization of various low molecular weight compounds with trityl (-CPh_3) groups promotes the ability of these materials to form a stable amorphous phase.[21–23]

Phosphorescent 2-arylbenzo[d]thiazole ligand containing iridium(III) complexes described in literature[24–26] were used as the core structures in order to obtain effective solution-processable amorphous phase forming OLED emitters. Trityl-functionalized 2-arylbenzo[d]thiazole ligands **2**, **5** and **8** were first obtained as the complexing compounds (Scheme 2.1). The ligands were used in further synthesis by first preparing di-μ-chloro iridium(III) complex dimers and then adding picolinic acid (complexes **3a**, **6a** and **9a**) or acetylacetone (complexes **3b**, **6b** and **9b**) ancillary ligands, respectively.

The obtained compounds exhibit high solubility in various volatile organic solvents such as DCM, chloroform and THF. Amorphous thin films could be prepared easily from the corresponding solutions using the spin coating method. The glass transition temperatures of the synthesized compounds determined by the differential scanning calorimetry (DSC) method vary in the range from 124 °C to 188 °C. No signs of crystallization of the materials were observed during several heating-cooling cycles.

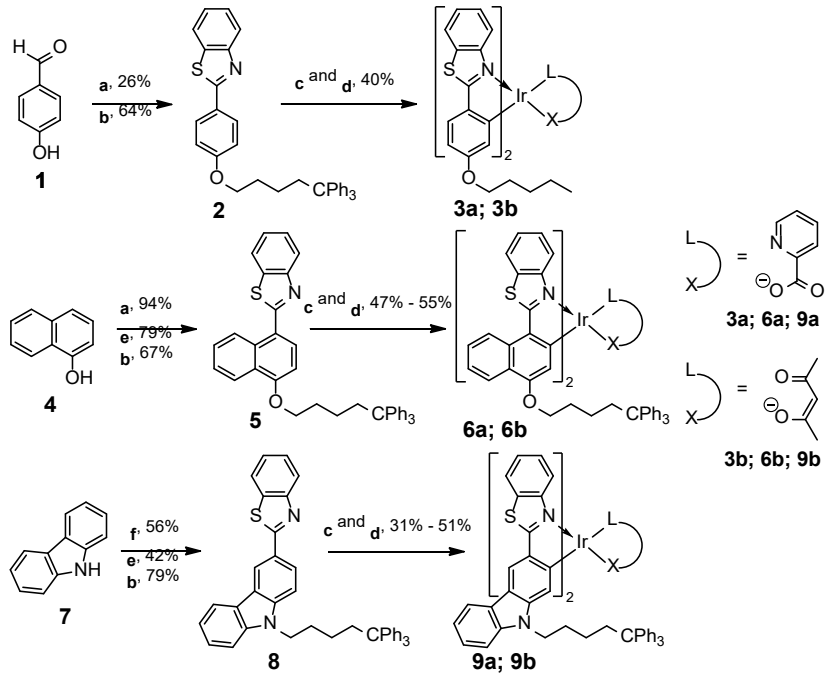

Scheme 2.1. Synthesis of the 2-arylbenzo[d]thiazole ligand containing iridium(III) complexes. (**a**) 1,1,1-Triphenyl-5-iodopentane, K_2CO_3, DMSO; (**b**) 2-aminothiophenol, DMSO; (**c**) $IrCl_3 \cdot 3H_2O$, 2-ethoxyethanol/H_2O; (**d**) acetylacetone or 2-picolinic acid, 2-ethoxyethanol, K_2CO_3; (**e**) $POCl_3$, DMF; (**f**) 1,1,1-triphenyl-5-iodopentane, NaH, THF.

The UV-Vis absorption patterns of the trityl-functionalized iridium(III) complexes are similar to the non-functionalized structural analogues described in the literature.[24–26] The highest energy UV-Vis absorption bands are attributed to metal-ligand charge transfer (MLCT) (Table 2.1). The largest bathochromic shift of absorption bands within the series is observed for complexes **6a** and **6b** containing 2-(naphthalen-1-yl)benzo[d]thiazole ligands. All

compounds exhibit intense phosphorescence with pronounced vibrational substructure, indicating that the emission is strongly associated with ligand-centred $^3\pi\rightarrow\pi^*$ transitions. Similarly to the UV-Vis absorption, complexes **6a** and **6b** have the largest bathochromic shift of the emission with orange-red phosphorescence, while complexes **3a**, **3b**, **9a**, and **9b** exhibit phosphorescence in the yellow part of the spectrum.

Measurements of the Φ_{PL} for both phosphorescent and TADF materials must be performed under degassed, oxygen-free conditions, as oxygen quenches the excited triplet states, thereby lowering the determined Φ_{PL} value.[27, 28] The compounds exhibit high Φ_{PL} in dilute solutions (0.64 to 0.90 in THF solution). In contrast, Φ_{PL} for amorphous thin films of pure emitters (without host matrix) drops to range 0.02–0.10. In this case, if the inert non-emissive 5,5,5-triphenylpentyl groups are not taken into account, the mass concentration of the active emitter in the thin amorphous films is approximately 50 wt %, which leads to a significant aggregation-induced quenching of the emission. During the preparation of the OLED active layer, the emitter is practically always mixed in a host matrix with emitter mass concentration lower than 10 wt %. Therefore, it was decided to determine the Φ_{PL} for thin amorphous films of guest-host systems with CBP and PVK. The inert 5,5,5-triphenylpentyl groups make up about half of the molecular weight of the compounds. For this reason, the complexes were mixed into the matrices at 20 wt % concentration, ensuring approximately 10 wt % concentration of the active emitter. In the CBP matrix, Φ_{PL} values reach 0.50. On the other hand, in the PVK matrix the values of Φ_{PL} are low and do not significantly differ from the Φ_{PL} of neat amorphous samples, what could be related to the increased aggregation of the emitter in the polymer type PVK matrix. In addition, a tendency of complexes containing picolinic acid ancillary ligands to exhibit a higher Φ_{PL} than the complexes containing acetylacetone ancillary ligands was observed.

Table 2.1

Photophysical Properties of Iridium(III) Complexes Containing 2-arylbenzo[d]thiazole Ligands

Comp.	$\lambda_{max\ abs}$ [a], nm (lg ε)	$\lambda_{max\ em}$ [b], nm	Φ_{PL} [c]	τ [d], μs	k_r [d], $\times10^5$ s^{-1}	k_{nr} [d], $\times10^5$ s^{-1}
3a	433 (3.7)	537, 576 (544, 576)	0.87/0.10/0.06/0.39	4.48	1.78	1.44
3b	464 (3.8)	552, 588 (553, 591)	0.78/0.02/0.15/0.31	3.32	1.56	0.45
6a	485 (4.3)	591, 641 (598, 644)	0.64/0.04/0.08/0.50	5.63	1.10	0.68
6b	496 (4.1)	595, 648 (604, 651)	0.64/0.03/0.06/0.27	3.75	1.15	2.49
9a	456 (4.0)	549, 588 (556, 587)	0.90/0.05/0.02/0.50	3.65	2.05	0.67
9b	464 (3.9)	568, 603 (568, 603)	0.69/0.02/0.02/0.12	2.61	1.34	1.52

[a] Maxima of the lowest energy absorption band, THF solution. [b] Phosphorescence, THF solution (CBP film, 20 wt % concentration). [c] THF solution/pure amorphous film/PVK film (20 wt % concentration)/CBP film (20 wt % concentration). [d] PMMA film (1 wt % concentration).

Complexes **9a** and **9b** containing the carbazole fragment were used in the fabrication of OLEDs (Dr. phys. A. Vembris). OLEDs were prepared using the following structure: ITO/PEDOT:PSS (40 nm)/emitting layer (60 nm)/BPhen or TPBi (20 nm)/LiF (1 nm)/Al. The

hole-transporting PEDOT:PSS and the emitting layers were fabricated using the spin coating method, while the electron-transporting BPhen/TPBi, the electron-injection LiF layers and the aluminium electrode were fabricated by the vacuum deposition. The maximal performance parameters were achieved for the **9a**/CBP based device, with 7.9 % external quantum efficiency, 12.4 cd·A^{-1} current efficiency and 7.8 lm·W^{-1} power efficiency at 6000 cd·m^{-2} luminance, with a maximum luminance of 17451 cd·m^{-2} (Table 2.2). Like in the case of Φ_{PL} measurements, lower performance parameters are observed for devices using PVK matrix and complex **9b** containing acetylacetone ancillary ligand.

Table 2.2

Electroluminescence Characteristics of **9a-b** Based OLEDs

Emitting Layer [a]	V_{on} [b], V	L_{max}, cd·m^{-2}	η_{ext} [c], %	η_c [d], cd·A^{-1}	η_p [e], lm·W^{-1}	λ_{max}, nm
9a:PVK	6.5	3229	4.8/4.8 [f]	7.2/7.2 [f]	4.5/4.5 [f]	553
9a:CBP	5.5	17451	7.9/5.1	12.4/8.0	7.8/5.6	554
9b:PVK	7.0	1708	2.1/1.7	3.1/2.4	1.9/1.3	561
9b:CBP	6.5	7295	5.2/5.1	7.3/7.1	4.9/4.7	563

[a] The mass concentration of iridium(III) complexes in the emitting layer is 20 wt %. [b] Voltage at which the luminance of the device is 1 cd·m^{-2}. [c] OLED external quantum efficiency. [d] Current efficiency. [e] Power efficiency. [f] Maximum achieved values and values determined at 1000 cd·m^{-2}.

The OLED performance parameters of the trityl-functionalized iridium(III) complexes are higher if compared to other structurally similar yellow emitters described in the literature, where the emitting layer is deposited by the spin coating method.[29, 30] However, the obtained results and literature analysis show that in terms of performance OLEDs produced by solution methods fall behind those produced by vacuum methods.[31, 32] Furthermore, the introduction of inert insulating groups such as long alkyl chains, which should reduce aggregation-induced quenching of the excited states, not necessarily leads to improved OLED performance.[33] These results prompted us to conduct a systematic study for the determination of the effect of trityl groups on the OLED performance.

In order to achieve this goal, compounds **15a**, **15b**, and **15c** based on the widely used OLED emitter **Ir(ppy)$_3$**[34] were synthesized with one, two, and three attached trityl groups, respectively (Scheme 2.2). For this purpose, di-μ-chloro dimers **13a** and **13b** were complexed with a third cyclometalating ligand using method developed by Colombo et al.[35] This method gives octahedral iridium(III) complexes in *fac* configuration. The target compounds were obtained through the reduction with $NaBH_4$ of one, two, and three aldehyde groups-containing complexes **14a**, **14b**, and **14c** and subsequent esterification of the obtained alcohols with 3,3,3-triphenylpropanoic acid.

The obtained trityl-functionalized compounds are soluble in volatile organic solvents, and spin coating method can be used for the preparation of high-quality thin amorphous films. The glass transition temperatures of compounds **15a**, **15b**, and **15c** are 158 °C, 142 °C, and 131 °C,

respectively. The decrease in the glass transition temperature in the series could be related to the increase in conformational freedom with the increase in the number of the trityl groups.

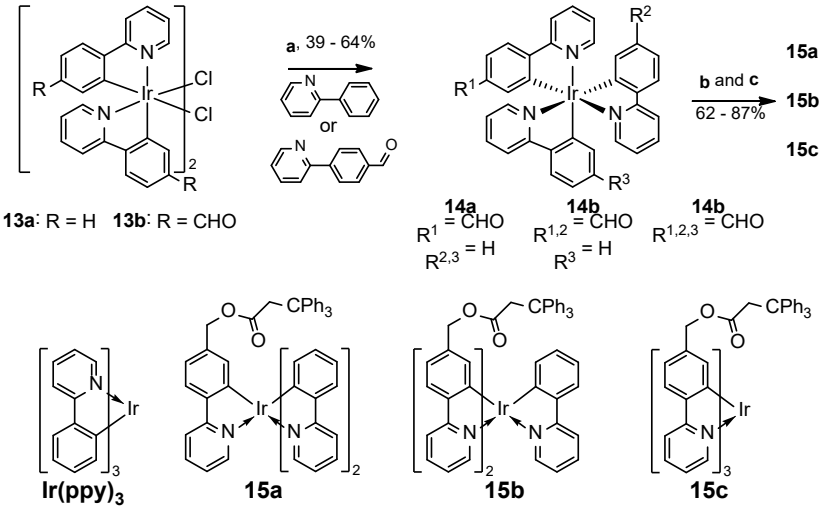

Scheme 2.2. Synthesis of trityl-functionalized Ir(ppy)$_3$ derivatives:
(**a**) AgOTf, diglyme; (**b**) $NaBH_4$, CH_2Cl_2/MeOH; (**c**) CPh_3CH_2COOH, DCC, DMAP, CH_2Cl_2.

No significant influence of the trityl groups on absorption and emission properties of compounds in solution was observed within the series (Table 2.3). Φ_{PL} in THF solutions is high, reaching values between 0.90 and 0.94. Φ_{PL} for amorphous thin films of pure emitters drops to 0.01–0.08, indicating an intensive aggregation of compounds in the solid state. Although compound **15c** has three attached trityl groups, due to the *fac* configuration the ligands align the trityl groups spatially in the same direction, covering only one side of the molecule. This allows us to hypothesize that weakly emitting dimers of complex molecules are formed as a result of aggregation.

Table 2.3

Photophysical Properties of Trityl-functionalized Ir(ppy)$_3$ Derivatives

Comp.	$\lambda_{max\ abs}$ [a], nm	$\lambda_{max\ em}$ [b], nm	Φ_{PL} [c]	τ [d], μs	k_r [d], $\times 10^5$ s^{-1}	k_{nr} [d], $\times 10^5$ s^{-1}
Ir(ppy)$_3$	379	522	0.94/-	1.7	5.5	0.35
15a	380	525	0.91/0.01	1.8	5.1	0.50
15b	379	525	0.90/0.03	1.7	5.3	0.58
15c	379	525	0.93/0.08	1.8	5.2	0.38

[a] Absorption, THF solution. [b] Phosphorescence, THF solution. [c] THF solution/pure amorphous film. [d] THF solution.

The electroluminescence properties of the obtained complexes were studied (Dr. phys. A. Vembris) using the following OLED structure: ITO/PEDOT:PSS (40 nm)/emitting layer (50 nm)/TPBi (20 nm)/LiF (1 nm)/ Al. Three types of host matrices were used for the

fabrication of the emitting layer – first, a pure hole-transporting PVK matrix, second, a mixture of PVK and electron-transporting OXD-7 in a 7:3 mass ratio, and third, a mixture of PVK and OXD-7 in a 3:7 mass ratio. Iridium(III) complexes were mixed into the matrix at a constant concentration of 7 wt %, attributing the mass of the inert trityl groups to the mass of the matrix. The emissive layer was prepared by the spin coating method. The obtained results (Table 2.4) show that unmodified **Ir(ppy)$_3$** outperforms trityl-functionalized compounds in terms of OLED performance parameters. Moreover, as the number of trityl groups in the molecule increases, the performance parameters of the OLEDs have tendency to decrease. It was hypothesized that the inert trityl groups interfere with the charge carrier transfer to the emitter molecules, thereby reducing the effectiveness of electroluminescence. For this reason, the compound **Ir(ppy)$_3$** with the least sterical hindrance by the bulky inert groups for the interaction with the charge carrier matrix exhibits the most efficient electroluminescence. Based on these results, it can be concluded that passive insulating groups should not be used for the purpose of aggregation limitation in solution-processable OLED. Peripheral groups with good charge transport properties, and appropriate energy level tuning could be proposed as a better alternative.

Table 2.4

Electroluminescence Characteristics of Trityl-functionalized Ir(ppy)$_3$ Derivatives

Emitting Layer [a]	V_{on} [b], V	L_{max}, cd·m^{-2}	η_c [c], cd·A^{-1}	η_p [d], lm·W^{-1}	*Roll-Off* [e], %
PVK					
Ir(ppy)$_3$	4.5	2446	6.8	3.9	44
15a	4.5	844	4.8	2.4	71
15b	6	127	1.6	0.6	-
15c	7	136	1.0	0.3	-
PVK:OXD-7 (7:3)					
Ir(ppy)$_3$	3.5	2983	7.8	4.4	6
15a	4	3308	6.9	3.7	10
15b	4	2692	7.3	3.9	27
15c	3.5	1794	6.6	3.8	10
PVK:OXD-7 (3:7)					
Ir(ppy)$_3$	3.5	1048	2.2	1.1	27
15a	3.5	638	2.0	1.0	23
15b	3.5	680	2.4	1.3	28
15c	4	560	2.2	1.3	25

[a] The mass concentration of iridium(III) complexes in the emitting layer is 7 % (mass of the inert trityl groups is attributed to the mass of the matrix). [b] Voltage at which the luminance of the device is 1 cd·m^{-2}. [c] Current efficiency. [d] Power efficiency. [e] Decrease in current efficiency from peak current efficiency to peak luminance.

The publications that cover the studies described in this chapter are given in Appendices 1 and 2.

3. Synthesis and TADF Properties of Carbene–metal–amide Complexes

Due to the high cost of rare transition metals (Ir, Pt, etc.) and environmental concerns, a possible replacement of phosphorescent emitters with TADF materials have been proposed in the recent years. In order to achieve lower ΔE_{ST} and promote rapid RISC, the most commonly applied TADF molecular design strategy involves the spatial separation of the donor (D) and acceptor (A) fragments, minimizing HOMO and LUMO overlap.[36] However, weak spin-orbit coupling leads to a slow RISC and low radiative rates.[37] Carbene-metal-amide (CMA) complexes are considered as a new class of TADF materials. In CMAs the d^{10} metal (Cu, Ag or Au) atom forms a linear complex with an electron-accepting *N*-heterocyclic carbene (NHC) ligand and an electron-donating amide ligand. This ligand configuration provides effective spatial separation of the frontal molecular orbitals, reducing ΔE_{ST}. The metal atom facilitates the spin-orbit coupling necessary for fast RISC. Therefore it is possible to realize TADF with high Φ_{PL} and photoluminescence lifetime below 1 µs. As a result, CMA emitters in OLED devices show performance parameters comparable to phosphorescent emitters.[38–41]

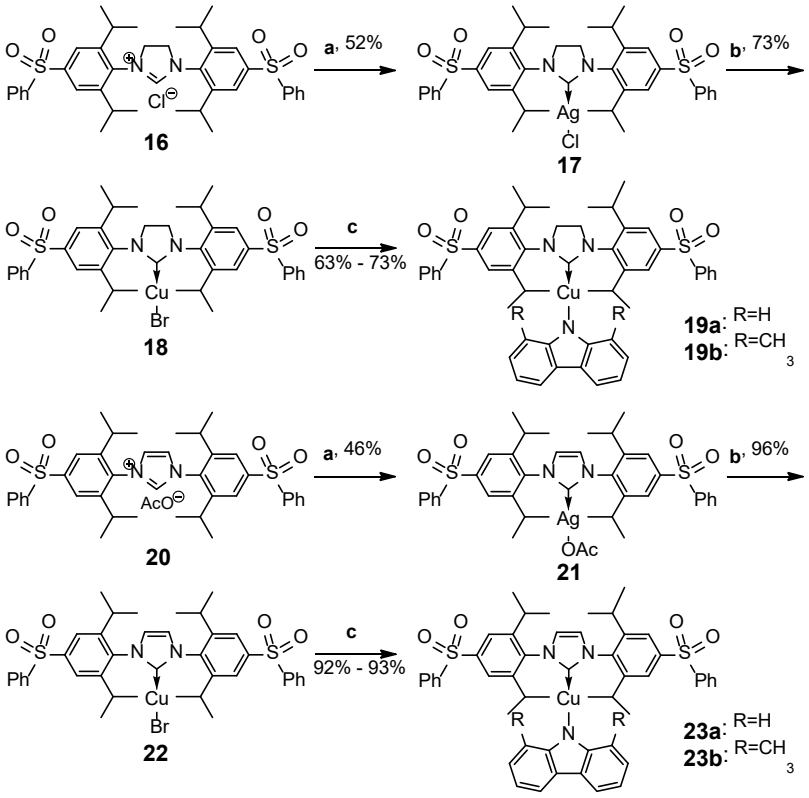

Scheme 3.1. Synthesis of Cu(I) CMA derivatives functionalized with phenylsulfonyl groups: (**a**) Ag_2O, MeCN; (**b**) CuBr, CH_2Cl_2; (**c**) derivative of carbazole, KO*t*Bu, THF.

A series of CMA type complexes was synthesized within the scope of this Doctoral Thesis with phenylsulfonyl acceptor groups added to the 4- position of 2,6-diisopropylphenyl (Dipp)

groups of the imidazole type NHC derivatives. The 4,5-dihydro-1*H*-imidazolium and 1*H*-imidazolium salts **16** and **20** required for the synthesis of NHC derivatives were obtained using a modified method described in the literature.[42] Silver(I) complexes **17** and **21** were obtained in the reaction of compounds **16** and **20** with Ag_2O. The silver atom was replaced by copper in a transmetalation reaction with CuBr, yielding copper(I) complexes **18** and **22**. CMA complexes **19a**, **19b**, **23a**, and **23b** were afforded in the reaction of Cu(I) complexes and deprotonated carbazole (Cbz) or 1,8-dimethylcarbazole (MeCbz).

In order to determine the effect of the metal atom on the luminescence properties of the phenylsulfonyl-functionalized CMA emitters, the analogue of complex **19a**, complex **25** was obtained with copper atom replaced by a gold atom (Scheme 3.2). The precursor **24** required for the synthesis of complex **25** was synthesized by transmetalation of silver(I) complex **17** with $AuCl{\cdot}Me_2S$.

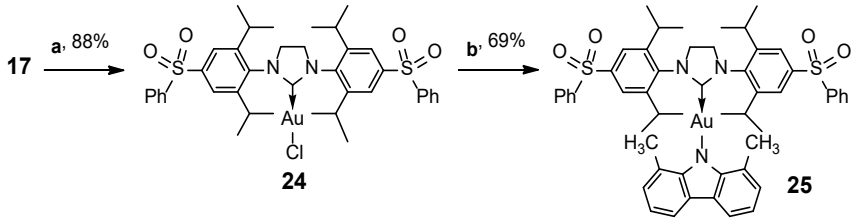

Scheme 3.2. Synthesis of phenylsulfonyl-functionalized Au(I) CMA derivative **25:**
(**a**) $AuCl{\cdot}Me_2S$, DCM; (**b**) derivative of carbazole, KO*t*Bu, THF.

The series was further extended by the synthesis of unsymmetrical complexes **28a** and **28b**. In these compounds only one of the Dipp groups has the phenylsulfonyl substitution (Scheme 3.3). Copper(I) complex **27** was obtained from 4,5-dihydro-1*H*-imidazolium chloride **26** in one step using the procedure developed by Santoro et al.[43] This method eliminates the requirement to obtain the silver(I) complex first and then use it in the following transmetalation reaction.

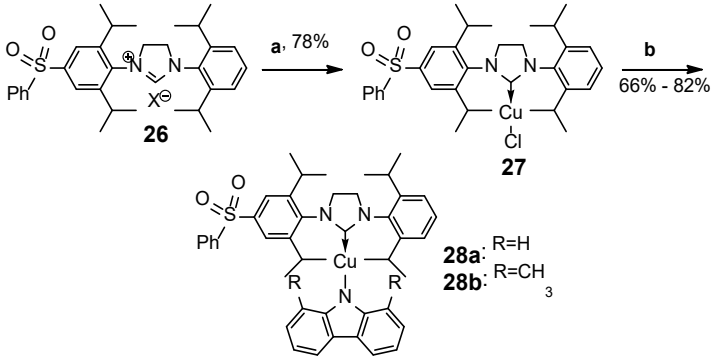

Scheme 3.3. Synthesis of unsymmetrical Cu(I) CMA derivatives functionalized with phenylsulfonyl group:
(**a**) CuCl, K_2CO_3, acetone; (**b**) derivative of carbazole, KO*t*Bu, THF.

The final complexes were afforded as white or slightly yellowish crystalline powders. In the solid state the compounds are stable in air and show no signs of decomposition after several months of storage. Complexes tend to decompose in solvents in the presence of proton donors (e.g., H_2O, HCl, etc.). The unsymmetrical complexes **28a** and **28b** containing one phenylsulfonyl group exhibit better solubility in non-polar solvents than the symmetric ones. The structures of compounds **19a**, **23b**, and **28a** in the crystalline state were characterized by X-ray crystallography (Fig. 3.1). The most significant structural variations were induced by different amide ligands. For compounds **19a** and **28a** (with a Cbz ligand), the Cu(I) metal coordination has a linear geometry with a slight bend at the metal centre (∡α) and a slight shift from the planar sp^2 geometry (∡β) at the carbazolide N atom. In these compounds the planes of Cbz and imidazolidine fragments are practically coplanar. Due to the steric effect of the methyl groups of MeCbz ligand, a significant shift from the linear geometry can be observed in compound **23b**, which is manifested as a pyramidalization of the carbazolide N atom (∡β = 147.3°). As a result, the alignment of the MeCbz ligand and Dipp cycle planes approaches coplanar (∡γ = 43.4°).

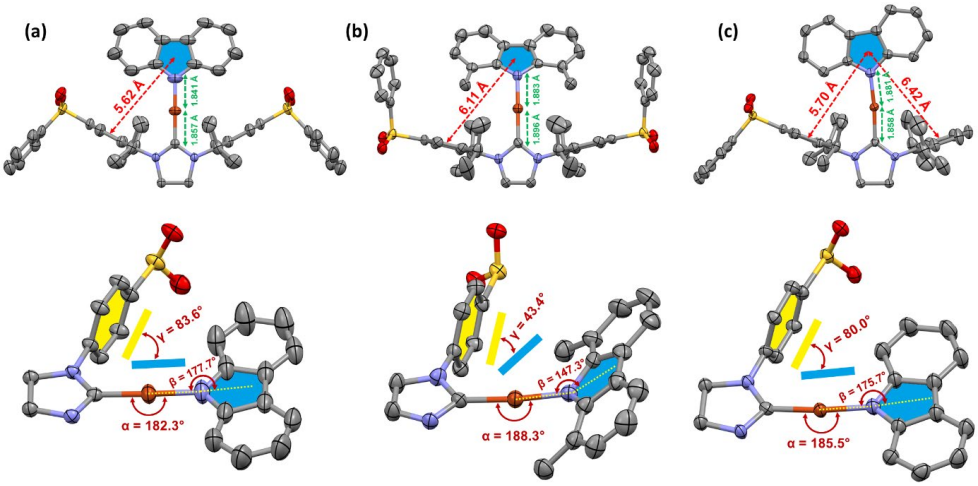

Fig. 3.1. X-ray structures of compounds **19a** (a), **23b** (b), **28a** (c) and the main structural parameters.

Time-dependent DFT (TD-DFT) calculations show that for all compounds in the series, the HOMO is located on the carbazolide ligand and has a small contribution from the metal atom (Fig. 3.2 (a)). The LUMO is located on the diphenylsulfone group. No contribution from either the central carbene ring or the metal atom to the LUMO was observed, marking a significant difference from the CMA emitters reported in the literature.[44–46] The orthogonal arrangement of the frontier molecular orbitals leads to a negligible overlap between the HOMO and LUMO.

The lowest energy singlet transition ($S_0 \rightarrow S_1$) takes place via through-space ligand-ligand charge transfer (LLCT) mechanism (Fig. 3.2 (c)). The calculated oscillator strength of the $S_0 \rightarrow S_1$ transition is low (in the range of 0.0021–0.0069). For the complexes with the MeCbz ligand, the $S_0 \rightarrow S_1$ transition is expected to have a higher oscillator strength than for the

complexes with the Cbz ligand, attributed to the decrease of angle γ between the donor carbazole and the acceptor Dipp planes (Fig. 3.1). Since the frontal molecular orbitals are spatially separated, the expected energy difference between the S_1 and T_1 states is low (ΔE_{ST} = 0.007–0.021 eV). The SOC between the S_1 and T_1 states is lower than that of other CMA complexes due to the negligible contribution of the metal atom to the LUMO orbital (Fig. 3.2 (b)).[47] However, even a small SOC can provide fast RISC considering the low ΔE_{ST} values.[48]

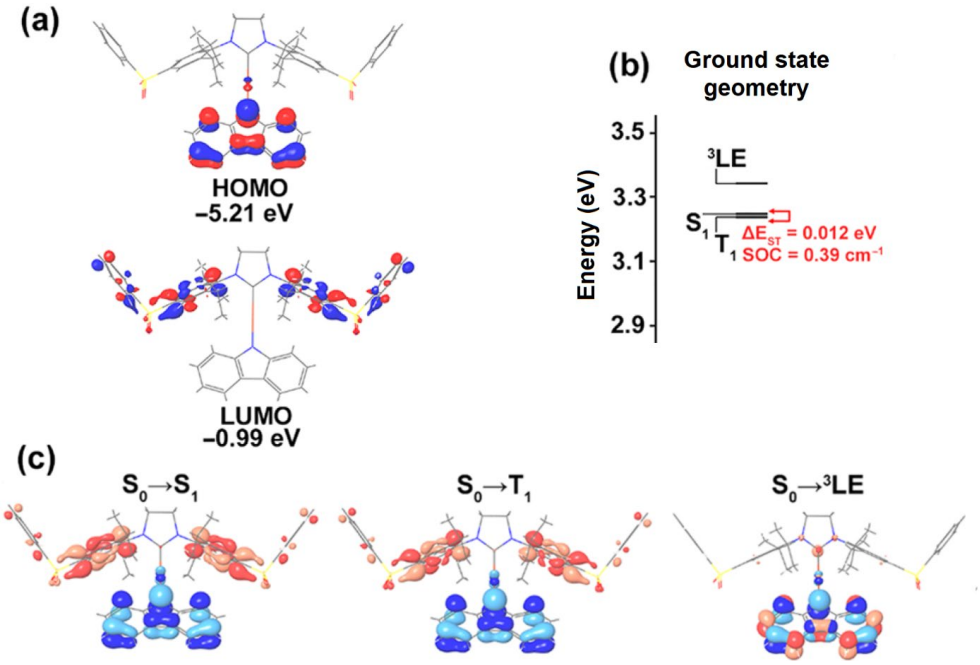

Fig. 3.2. (a) HOMO and LUMO orbitals for compound **19a**. (b) Energy diagram of the lowest energy excited states. (c) Natural transition orbitals.

A similar UV-Vis absorption pattern is observable for all compounds in the series. Several structured absorption bands can be observed in the 300–380 nm region. The position and shape of the structured absorption bands are not affected by changes of solvent polarity (Fig. 3.3 (a)). These absorption bands are attributed to local π–π* transitions of the carbazolide ligand. The CT transition in these compounds is shown as a broad absorption band of weak intensity, which extends up to 450 nm in less polar solvents. The LLCT nature of this absorption band is confirmed by the hypsochromic shift observed with increasing solvent polarity.[40] Accurate determination of the intensity of the CT band is difficult due to the overlap with the π–π* absorption bands of the carbazolide ligand. The extinction coefficient of the CT absorption band can be roughly estimated in the range of 1000 $M^{-1}cm^{-1}$ to 3000 $M^{-1}cm^{-1}$ in toluene solutions. Within the series the compounds with MeCbz ligand exhibit more intensive CT absorption than the compounds with Cbz ligand, confirming the predictions of TD-DFT calculations.

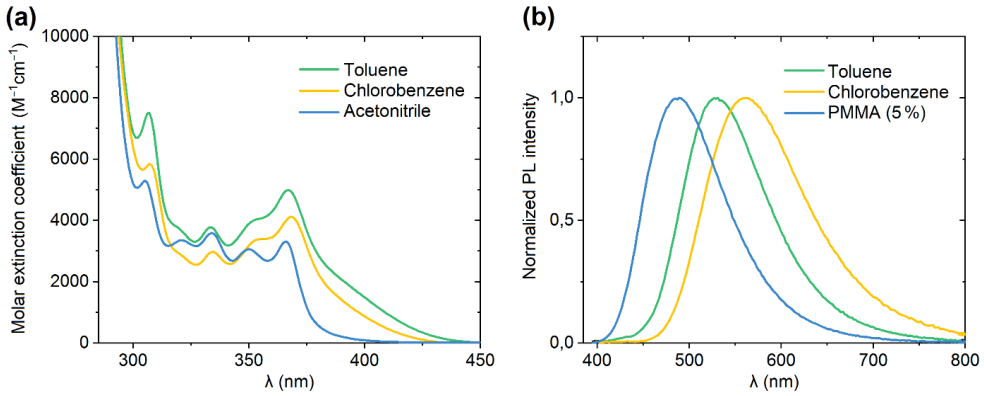

Fig. 3.3. (a) UV-Vis absorption of compound **19b** in different solvents (10^{-5} M). (b) Photoluminescence of compound **19b** in toluene, chlorobenzene (10^{-5} M) and PMMA (5 wt %).

The compounds have similar emissive properties in toluene solutions (Table 3.1). The complexes in toluene exhibit emission from the CT excited state with a maxima at 519–547 nm. A bathochromic shift is observed for the CT emission band as the polarity of the solvent increases (Fig. 3.3 (b)). The Φ_{PL} of the complexes in toluene solution does not exceed 0.39 due to the various possible vibrational relaxation processes. Similar to the phosphorescent iridium complexes, the Φ_{PL} of CMA complexes decreases in the presence of oxygen, indicating the involvement of triplet excited states in the emission mechanism.

Table 3.1

Emissive Properties of CMA Derivatives Functionalized with Phenylsulfonyl Groups

Comp.	$\lambda_{max\ em}$ [a], nm	Φ_{PL} [a]	$\lambda_{max\ em}$ [b], nm	Φ_{PL} [b]	τ_{prompt} [b], ns	τ_1 [b], μs	τ_2 [b], μs	k_r [b], $\times 10^5$ s^{-1}	k_{nr} [b], $\times 10^5$ s^{-1}
19a	523	0.31	472	0.86	6 (0.2 %)	2.5 (45.4 %)	10.6 (54.4 %)	1.25	0.20
19b	521	0.25	482	0.84	12 (0.4 %)	1.5 (61.6 %)	5.2 (38.0 %)	2.89	0.55
23a	547	0.21	488	0.90	10 (0.4 %)	2.0 (46.6 %)	8.3 (53.0 %)	1.68	0.19
23b	541	0.28	492	0.84	19 (0.8 %)	1.4 (59.8 %)	4.3 (39.4 %)	3.32	0.63
25	521	0.27	502	0.69	1 (0.2 %)	1.4 (31.8 %)	4.7 (68.0 %)	1.89	0.85
28a	519	0.38	464	0.80	19.4	2.3	9.9	-	-
28b	521	0.39	476	0.79	37.2 (0.7 %)	1.4 (44.3 %)	5.4 (55.0 %)	2.21	0.59

[a] Luminescence, toluene solution. [b] Luminescence, PMMA film (5 wt %).

In the solid state the molecular motion subsides and the Φ_{PL} of the complexes in thin amorphous films (PMMA, 5 % emitter mass concentration) increases significantly, reaching a maximum value of 0.90 for compound **23a**. In comparison to solutions, PMMA films show a hypsochromic shift of emission (rigidochromism[49]). The emission of compounds in PMMA films is characterized with a complex TADF mechanism with numerous variations within the series. All of the compounds exhibit three-exponential photoluminescence decay kinetics (Fig. 3.4 (a)). Prompt fluorescence (τ_{prompt} = 6 – 37 ns) is observed for the compounds due to the low rates of ISC. The contribution of the prompt fluorescence to the total photoluminescence intensity does not exceed 1 %. The intersystem crossing rate is reduced by the low SOC between the S_1 and T_1 states. Two delayed fluorescence components are observed for the compounds: the first with a lifetime (τ_1) in the range of 1.36 µs to 2.50 µs and the second with a lifetime (τ_2) in the range of 4.25 µs to 10.59 µs. The contribution of the two delayed fluorescence components to the total photoluminescence intensity is similar. The TADF nature of the delayed fluorescence was demonstrated by cooling the samples and observing a gradual decrease of the radiative rate (k_r). The experimentally determined TADF activation energy (ΔE_{ST}) of the compounds varies from 0.0068 eV to 0.0110 eV, which is in agreement with the values predicted by TD-DFT calculations. The dual nature of the TADF can be explained by emission from two different conformations of the molecule. Au(I) complex **25** should be mentioned as an exception. In the case of this compound the fastest component (τ_1) is TADF emission, while the slowest component (τ_2) is related to phosphorescence from the T_2 state, which is energetically close to the S_1 state. The combined radiative rate in the series varies from $1.25 \cdot 10^5$ s^{-1} to $3.32 \cdot 10^5$ s^{-1}. Due to the higher oscillator strength for the lowest energy CT transition, the complexes with the MeCbz ligand have larger k_r values than those with the Cbz ligand.

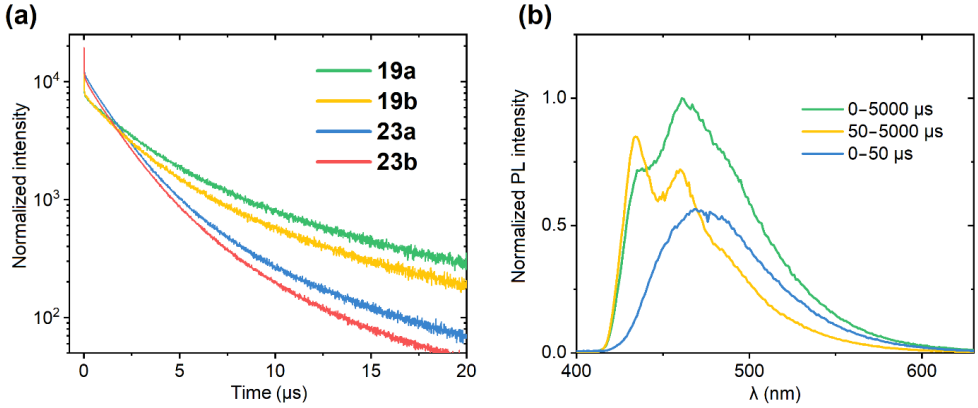

Fig. 3.4. (a) Photoluminescence kinetics of compounds **19a–b** and **23a–b** in PMMA. (b) Time-dependent photoluminescence of compound **19b**, PMMA film (5 wt %.) at 77 K.

In addition to TADF and possible phosphorescence from the T_2 state (compound **25**), the emission from the carbazolide local triplet excited state (^{3}LE) should be considered as well. Compared to TADF, this emission has a very long lifetime (from several hundreds to a few

thousand microseconds), and time-resolved emission spectroscopy can be used to resolve this luminescence component (Fig. 3.4 (b)). The emission from ^{3}LE state exhibits a fine structure characteristic to the phosphorescence of carbazole derivatives.[41] In the case of compound **23a** (PMMA film), ^{3}LE phosphorescence of carbazolide ligand is observable at room temperature, while for the other compounds in the series it only appears when the samples are cooled. According to TD-DFT calculations, the ^{3}LE state is relatively close in energy to the S_1 state. Upon cooling the samples, the rigidification of PMMA matrix takes place, which destabilizes the S_1 state associated with the LLCT process. As a result, the energy of S_1 state can approach or even exceed the ^{3}LE state, making phosphorescence from the ^{3}LE excited state possible.

Although the new compounds belong to the class of CMA emitters structurally, the luminescence mechanisms differ significantly. In this case, TADF proceeds via through-space CT mechanism. Emitters therefore have very low ΔE_{ST} values, and a small SOC provided by the metal atom promotes RISC. As a result, the achieved Φ_{PL} and radiative rates are comparable to the currently best emitters of the CMA class.[50] From the point of photophysical functionality, the carbene cycle in the new compounds is an inert linking fragment between the donor and acceptor fragments.

In order to evaluate the electroluminescence properties of the compounds, complex **23b** was used to prepare an OLED (Dr. phys. A. Vembris) with the following structure: ITO/PEDOT:PSS (40 nm)/PolyTPD (30 nm)/**23b** (20 wt %): CzSi (40 nm)/TPBi (40 nm)/LiF (1 nm)/Al (100 nm). The emissive layer was prepared from compounds in a solution using the spin coating method. The device showed 6 V turn-on voltage, 1.7 cd/A current efficiency, 0.6 lm/W power efficiency, and 0.8 % external quantum efficiency. The electroluminescence spectrum of the device indicates emission from the CT state of the complex. The obtained results demonstrate the suitability of the compounds for the preparation of electroluminescent devices; however, further optimization is required to improve the performance of the devices.

In the last section of the Doctoral Thesis, the photophysical and electroluminescence properties of CMA derivatives based on 1,3-thiazol-2-ylidene carbene fragment were studied. The 1,3-thiazolium perchlorate salts **29**–**31** known in literature[51] were used as starting materials for the synthesis of the target compounds (Scheme 3.4). Carbene-Cu-Cl complexes were synthesized by *in situ* generation of free carbenes from perchlorate salts in the presence of CuCl. The carbene-Cu-Cl complexes were further used in the synthesis of CMA derivatives. A series of eight compounds were obtained by utilizing different carbazole derivatives as ligands: **32a**, **33a**, and **34a** with carbazole (Cbz) ligand, **32b**, **33b**, and **34b** with 1,8-dimethylcarbazole (MeCbz) ligand, **34c** with 3,6-di-*tert*-butylcarbazole (*t*BuCbz), and **34d** with a 3,6-di-*tert*-butyl-1,8-dimethylcarbazole (Me*t*BuCbz) ligand. The compounds are stable in the solid state and can be stored in air. Complexes exhibit moderate solubility in organic solvents such as toluene, chlorobenzene, dichloromethane and THF. The solubility of compounds is significantly improved by *tert*-butyl groups. An interesting exception is compound **34b**, which has very low solubility in organic solvents at room temperature.

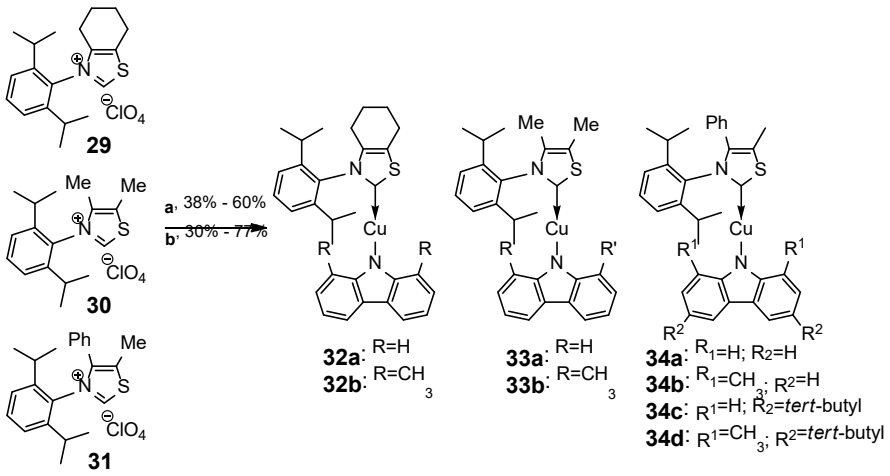

Scheme 3.4. Synthesis of Cu(I) CMA derivatives based on 1,3-thiazol-2-ylidene carbene fragment.

(**a**) CuCl, NaO*t*Bu, THF; (**b**) derivative of carbazole, KO*t*Bu, THF.

The compounds exhibit a practically linear geometry at the complex-forming metal atom and a coplanar arrangement of the carbazolide and carbene rings (Fig. 3.5). Various structural deformations are introduced by the substitution at the carbazolide ligand (1,8-dimethyl groups) and the 1,3-thiazol-2-ylidene ring (4-phenyl group). The steric effects of the 1,8-dimethyl groups of the carbazolide ligand cause repulsion from the Dipp group, turning ∡α towards the unhindered sulphur atom. The Cu-N and Cu-$C_{carbene}$ bonds are lengthened as well. The 4-phenyl group at the carbene ring causes the twist of the Dipp (∡γ) and carbazolide (∡β) planes relative to the plane of the carbene ring. The respective sterical groups introduce not only structural deformations, but also reduce the conformational freedom of the molecule by limiting the rotational freedom of Dipp group, 4-phenyl group and the carbazolide ligand. The low solubility of compound **34b** could be directly related to the rigid molecular structure, which increases the tendency of the molecule to form poorly soluble crystals.

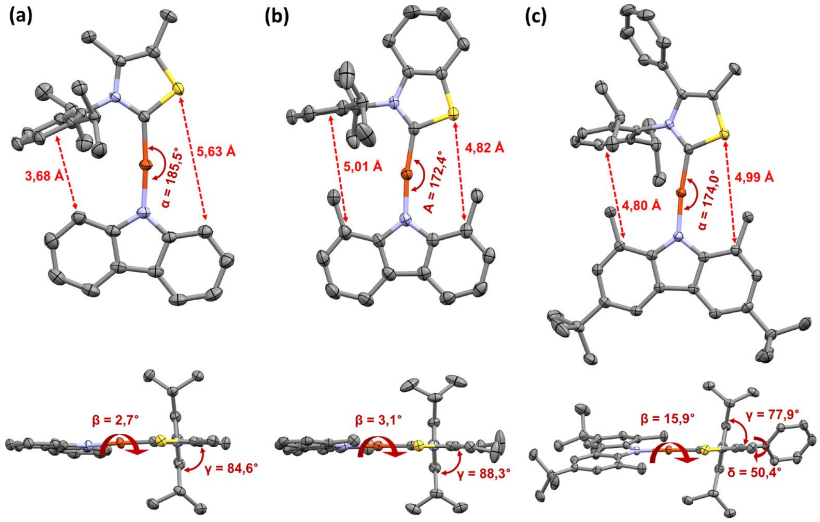

Fig. 3.5. X-ray structures of compounds **33a** (a), **32b** (b), and **34d** (c) and the main structural parameters.

Similarly to the phenylsulfonyl-functionalized CMAs, UV-Vis absorption bands attributed to the local π–π* transitions of the carbazolide ligand can be observed from 300 nm to 380 nm for 1,3-thiazol-2-ylidene derivatives in toluene solution (Fig. 3.6 (a)). The lowest energy absorption bands of the complexes correspond to the CT transition. The intensity of CT transition is significantly higher than that of the phenylsulfonyl-functionalized CMA derivatives, reaching a molar extinction coefficient of $8.0 \cdot 10^3$ $M^{-1} \cdot cm^{-1}$ in the case of compound **34c**. The position of the CT absorption maxima depends on the substituents of the carbazolide ligand. A slight bathochromic shift of the absorption peak is observed when weakly electron-donating methyl or *tert*-butyl groups are added to the carbazolide ligand. As in the case of other CMA type compounds, the CT absorption bands of the complexes shift hypsochromically with increasing solvent polarity.[40]

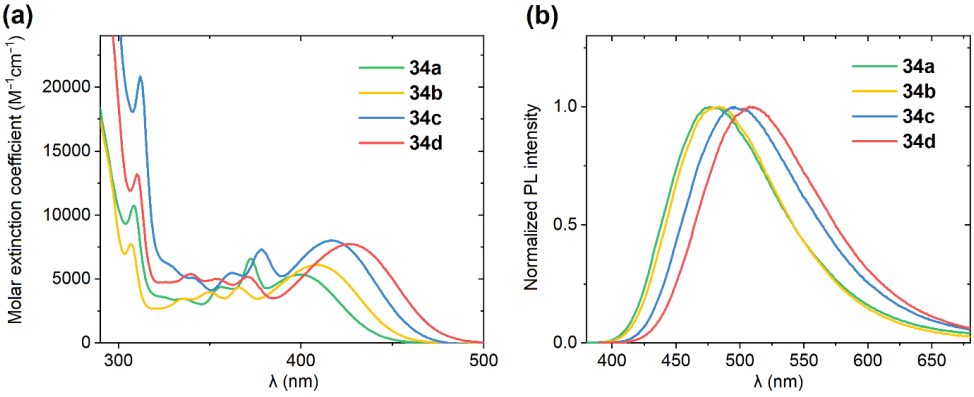

Fig. 3.6. (a) UV-Vis absorption of compounds **34a–d** in toluene (10^{-5} M).
(b) Photoluminescence of compounds **34a–d** in PMMA film (5 wt % concentration).

The luminescence properties of compounds in toluene solutions and thin amorphous films (PMMA, 5 % emitter mass concentration) are given in Table 3.2. The emission proceeds from the CT excited state. Just as the UV-Vis absorption, the position of the luminescence maxima depends on the substituents on the carbazolide ligand (Fig. 3.6 (b)). An increase of Φ_{PL} and a hypsochromic shift of the luminescence maxima can be observed in the solid state in comparison to the solutions. A correlation between the complex structure and k_r for thin amorphous film samples can be observed. Complexes with 1,8-dimethyl substituted carbazolide ligand exhibit k_r 1.1–1.6 times higher than structural analogues with 1,8-unsubstituted carbazolide. The highest k_r values were observed for complexes **34b** and **34d** with a 4-phenyl-substituted 1,3-thiazol-2-ylidene cycle in addition to the 1,8-dimethyl substituted carbazolide. Therefore, it can be concluded that limitations in the rotational freedom of the carbazolide ligand increase the k_r values.

Table 3.2

Emissive Properties of 1,3-thiazol-2-ylidene Carbene Cu(I) CMA Derivatives

Comp.	$\lambda_{max\ em}$[a], nm	Φ_{PL}[a]	$\lambda_{max\ em}$[b], nm	Φ_{PL}[b]	T[b], μs	k_r[b], $\times 10^5\ s^{-1}$	k_{nr}[b], $\times 10^5\ s^{-1}$
32a	511	0.37	471	0.74	2.6	2.8	1.0
32b	517	0.42	478	0.82	1.9	4.3	0.9
33a	507	0.41	467	0.68	1.9	3.6	1.6
33b	513	0.79	474	0.84	2.1	4.0	0.8
34a	521	0.39	479	0.71	2.1	3.4	1.4
34b	527	0.23	484	0.78	1.6	4.9	1.4
34c	549	0.73	499	0.73	1.6	4.6	1.7
34d	554	0.76	509	0.86	1.2	7.2	1.2

[a] Luminescence, toluene solution. [b] Luminescence, PMMA film (5 wt % concentration).

Compounds in PMMA films exhibit monoexponential photoluminescence decay kinetics with τ_{PL} ranging from 1.2 μs to 2.6 μs (Fig. 3.7 (a)). Upon cooling, all compounds in the series except for **34d** exhibit an emission from the local triplet excited state (^{3}LE) of the carbazolide ligand. Similarly to the phenylsulfonyl-functionalized CMAs, the luminescence from ^{3}LE state can be explained by the rigidification of the PMMA matrix and the resulting destabilization of the CT state. Compound **34d** is an exception because the energy level of the CT state is shifted too far from the energy level of the ^{3}LE state. Therefore, for compound **34d** only CT excited state emission is observable in the entire temperature range from RT to 10 K, with a hypsochromic shift with gradual cooling. An increase in τ_{PL} up to 140 μs at 10 K is also observed upon cooling (Fig. 3.7 (b)), which indicates the TADF nature of the CT emission. At room temperature TADF from the S_1 state is observed. The phosphorescence intensity from the T_1 state increases upon gradual cooling of the sample, until at 50 K the emission occurs only from the T_1 state. By fitting the temperature dependence of τ_{PL} to a modified Boltzmann equation[52] (Fig. 3.7 (b)), ΔE_{ST} was estimated at 0.044 eV for compound **34d**.

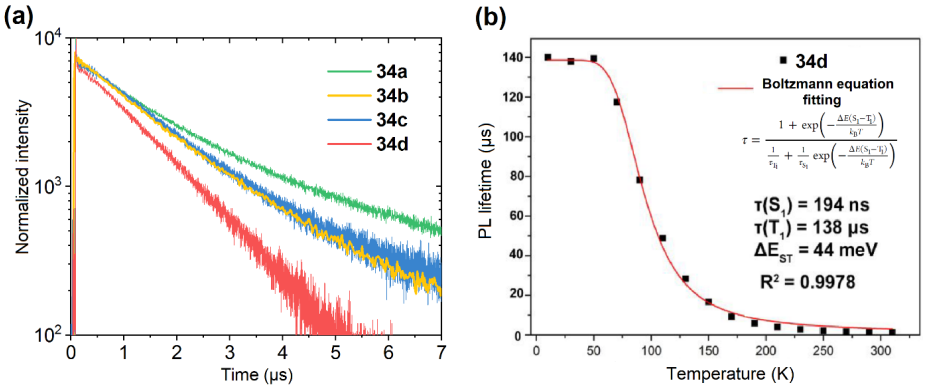

Fig. 3.7. (a) Photoluminescence decay kinetics of compounds **34a–d**, PMMA films (5 wt % concentration). (b) The temperature dependence of the photoluminescence lifetime of compound **34d** and fit against a modified Boltzmann equation, PMMA film (5 wt % concentration).

To investigate the luminescence mechanism and to characterize the influence of steric effects on the luminescence properties, TD-DFT calculations were performed for complexes **34a** and **34b** (Dr. chem. G. Baryshnikov). It was found that the HOMO is localized on the carbazolide ligand, while the LUMO is on the 1,3-thiazol-2-ylidene fragment (Fig. 3.8 (a)). Therefore, the transition to the S_1 excited state exhibit LLCT properties. Both the HOMO and LUMO have a small metal atom contribution, leading to an increase of the $S_0 \rightarrow S_1$ transition oscillator strength and increase of ΔE_{ST}.

According to TD-DFT calculations, the planes of the 1,3-thiazol-2-ylidene and carbazolide ligands are practically coplanar in the ground state S_0 and in the T_1 excited state. On the other hand, at the S_1 excited state these planes tend to rotate to an orthogonal position (Fig. 3.8 (b)), for **34a** assuming dihedral angle $\measuredangle\beta = 77°$. Meanwhile, the rotation of the carbazolide ligand in compound **34b** is hindered due to the steric interaction of 1,8-dimethyl and Dipp groups, so the dihedral angle is smaller ($\measuredangle\beta = 55°$). For this reason, the calculated oscillator strength of the $S_1 \rightarrow S_0$ transition for compound **34b** is two times larger that of **34a**, leading to an equal increase in the predicted delayed fluorescence rate. Thus, the interaction of sterically bulky groups increases the radiative rate in the series of 1,3-thiazol-2-ylidene CMA derivatives.

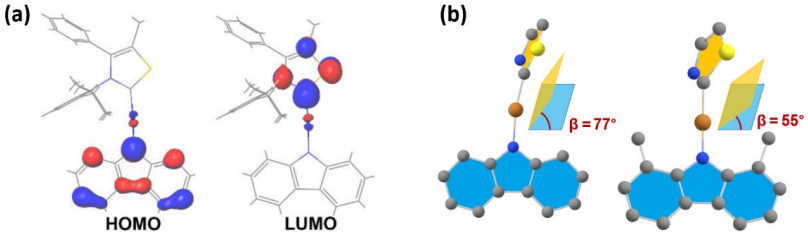

Fig. 3.8. (a) Geometry of HOMO and LUMO for compound **34a**, S_0 geometry. (b) Dihedral angles between the planes of the 1,3-thiazol-2-ylidene and carbazolide in compounds **34a** and **34b**, S_1 geometry.

Compound **34d** shows both the highest Φ_{PL} and the largest k_r in the solid state, therefore it was chosen together with the structural analogue **34c** for OLED preparation (Dr. C.H. Chang). mCBP was selected as the most effective emissive layer host matrix among the four tested materials (CBP, mCBP, mCP, and DPEPO). The following structure was used for the OLED preparation: ITO/TAPC (35 nm)/TCTA (5 nm)/emitting layer (25 nm)/TmPyPB (50 nm)/LiF (1.5 nm)/Al (150 nm) with 1 %, 5 %, 10 %, and 20 % emitter mass concentration in emitting layer. The emissive layer was prepared by the vacuum deposition method. The highest performance parameters were achieved for the device using compound **34c** as emitter, reaching 16.5 % external quantum efficiency and 44215 cd·m^{-2} luminance at 10 wt % emitter doping concentration (Table 3.3). Two distinct emission bands with maxima at 495 nm and 600 nm can be observed in the electroluminescence spectrum of compound **34c** (Fig. 3.9). As the emitter doping concentration increases, the relative intensity ratio between the emission bands at 495 nm and 600 nm increases in favour of the latter. The electroluminescence at 495 nm is recognized as the TADF emission of **34c**, while the electroluminescence at 600 nm could be related to the emission of dimers of compound **34c**, in other words, excimer electroluminescence. As a result, a very broad electroluminescence spectral profile is obtained, which is applicable for the production of white light OLEDs. For compound **34d**, excimer electroluminescence is observed to a much lesser extent than for **34c**. The steric effects induced by 1,8-dimethyl groups reduce the possibilities of compound **34d** to form dimers in the emitting layer.

Table 3.3

OLED Performance Parameters for Compounds **34c–d**

Emitting Layer	V_{on} [a], V	L_{max}, cd·m^{-2}	η_{ext} [b], %	η_c [c], cd·A^{-1}	η_p [d], lm·W^{-1}
34c:mCBP					
1 %	3.8	13542	10.3/7.0 [e]	22.7/15.4 [e]	19.8/9.3 [e]
5 %	3.6	17839	13.7/9.8	25.9/18.6	22.3/11.6
10 %	3.5	44215	16.5/16.1	34.1/33.1	27.1/23.6
20 %	3.7	41695	15.7/14.6	26.0/25.5	20.2/17.0
34d:mCBP					
1 %	3.7	35947	12.9/10.6	31.5/25.8	25.4/17.0
5 %	3.6	42773	12.2/11.6	31.9/30.4	26.0/20.4
10 %	3.8	36478	9.2/9.1	21.7/21.6	15.5/13.2
20 %	3.8	37183	5.9/5.8	14.8/13.4	9.4/8.6

[a] Voltage at which the luminance of the device is 1 cd·m^{-2}. [b] OLED external quantum efficiency. [c] Current efficiency. [d] Power efficiency. [e] Maximum achieved values and values determined at 100 cd·m^{-2}.

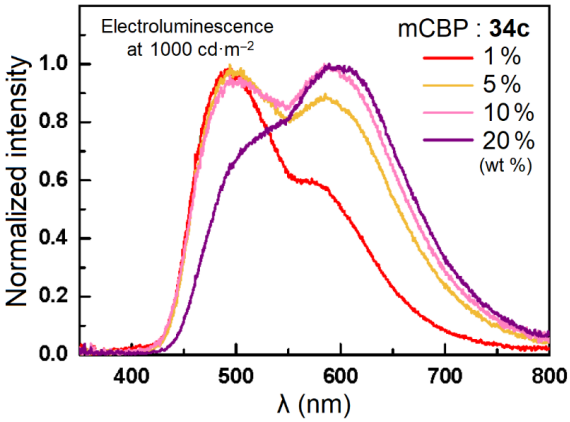

Fig. 3.9. Electroluminescence spectra of compound **34c** at 1000 cd·m^{-2} brightness.

The publications that cover the studies described in this chapter are given in Appendices 3–6.

CONCLUSIONS

1. The functionalization of organic emitters with trityl groups can be employed to obtain luminescent materials that form morphologically stable amorphous thin films from volatile organic solvents. Obtained compounds can be used for the production of OLED devices via the spin coating method.
2. Trityl groups obstruct the charge transfer to the emitter molecules, thus reducing the efficiency of electroluminescence.
3. The obtained phenylsulfonyl-functionalized and 1,3-thiazol-2-ylidene carbene based CMA type Cu(I) complexes exhibit solid state photoluminescence with high Φ_{PL} and a few microsecond lifetime.
4. For the phenylsulfonyl-functionalized CMA derivatives, TADF emission is related to a through-space charge transfer mechanism. Low ΔE_{ST} values in combination with the spin-orbit coupling provided by the metal atom contribute to efficient and fast emissive process.
5. Steric effects influence the photophysical properties of the studied CMA derivatives. In the series of phenylsulfonyl-functionalized CMA compounds, the steric effects of the 1,8-dimethyl groups of the carbazolide ligand lead to a more favourable spatial arrangement of the D and A fragments, thereby increasing the radiative rates. In the series of 1,3-thiazol-2-ylidene carbene based CMA derivatives, the radiative processes are promoted by the interaction of the sterically bulky groups that reduce the rotation of the carbazolide ligand in the S_1 excited state.
6. For the series of 1,3-thiazol-2-ylidene CMA derivatives, efficient excimer electroluminescence can be observed, which could be utilized for the preparation of white light OLEDs.

REFERENCES

[1] B. Geffroy, P. le Roy, C. Prat, *Polym. Int.* **2006**, *55*, 572–582.

[2] F. So, J. Kido, P. Burrows, *MRS Bull.* **2008**, *33*, 663–669.

[3] S. Wang, H. Zhang, B. Zhang, Z. Xie, W.-Y. Wong, *Mater. Sci. Eng. R Reports* **2020**, *140*, 100547.

[4] R. Karlicek, C. C. Sun, G. Zissis, R. Ma, *Handbook of Advanced Lighting Technology*, Springer International Publishing, Cham, **2017**.

[5] L. Duan, L. Hou, T.-W. Lee, J. Qiao, D. Zhang, G. Dong, L. Wang, Y. Qiu, *J. Mater. Chem.* **2010**, *20*, 6392–6407.

[6] Y. Zou, S. Gong, G. Xie, C. Yang, *Adv. Opt. Mater.* **2018**, *6*, 1800568.

[7] L. Xiao, Z. Chen, B. Qu, J. Luo, S. Kong, Q. Gong, J. Kido, *Adv. Mater.* **2011**, *23*, 926–952.

[8] Y. Im, M. Kim, Y. J. Cho, J. A. Seo, K. S. Yook, J. Y. Lee, *Chem. Mater.* **2017**, *29*, 1946–1963.

[9] C. W. Tang, S. A. VanSlyke, *Appl. Phys. Lett.* **1987**, *51*, 913–915.

[10] J. Bauri, R. B. Choudhary, G. Mandal, *J. Mater. Sci.* **2021**, *56*, 18837–18866.

[11] C. Zhong, C. Duan, F. Huang, H. Wu, Y. Cao, *Chem. Mater.* **2011**, *23*, 326–340.

[12] J.-H. Jou, S. Kumar, A. Agrawal, T.-H. Li, S. Sahoo, *J. Mater. Chem. C* **2015**, *3*, 2974–3002.

[13] T. Chatterjee, K.-T. Wong, *Adv. Opt. Mater.* **2019**, *7*, 1800565.

[14] H. Yersin, A. F. Rausch, R. Czerwieniec, T. Hofbeck, T. Fischer, *Coord. Chem. Rev.* **2011**, *255*, 2622–2652.

[15] K.-L. Wong, J.-C. G. Bünzli, P. A. Tanner, *J. Lumin.* **2020**, *224*, 117256.

[16] S. Ghosh, S. Mandal, C. Banerjee, V. G. Rao, N. Sarkar, *J. Phys. Chem. B* **2012**, *116*, 9482–9491.

[17] G. Hong, X. Gan, C. Leonhardt, Z. Zhang, J. Seibert, J. M. Busch, S. Bräse, *Adv. Mater.* **2021**, *33*, 2005630.

[18] K. Mori, T. P. M. Goumans, E. van Lenthe, F. Wang, *Phys. Chem. Chem. Phys.* **2014**, *16*, 14523–14530.

[19] M. Y. Wong, E. Zysman-Colman, *Adv. Mater.* **2017**, *29*, 1605444.

[20] T. Huang, W. Jiang, L. Duan, *J. Mater. Chem. C* **2018**, *6*, 5577–5596.

[21] K. Traskovskis, I. Mihailovs, A. Tokmakovs, A. Jurgis, V. Kokars, M. Rutkis, *J. Mater. Chem.* **2012**, *22*, 11268-11276.

[22] K. Traskovskis, K. Lazdovica, A. Tokmakovs, V. Kokars, M. Rutkis, *Dye. Pigment.* **2013**, *99*, 1044–1050.

[23] E. Zarins, K. Balodis, A. Ruduss, V. Kokars, A. Ozols, P. Augustovs, D. Saharovs, *Opt. Mater.* **2018**, *79*, 45–52.

[24] I. R. Laskar, T.-M. Chen, *Chem. Mater.* **2004**, *16*, 111–117.

[25] T. Giridhar, W. Cho, Y.-H. Kim, T.-H. Han, T.-W. Lee, S.-H. Jin, *J. Mater. Chem. C* **2014**, *2*, 9398–9405.

[26] J.-H. Jang, M. J. Kim, H. U. Kim, S. B. Lee, J. Lee, D.-H. Hwang, *J. Nanosci.*

Nanotechnol. **2016**, *16*, 8580–8584.
[27] X. Jiang, J. Peng, J. Wang, X. Guo, D. Zhao, Y. Ma, *ACS Appl. Mater. Interfaces* **2016**, *8*, 3591–3600.
[28] S. E. Zieger, A. Steinegger, I. Klimant, S. M. Borisov, *ACS Sensors* **2020**, *5*, 1020–1027.
[29] T. Giridhar, W. Cho, J. Park, J.-S. Park, Y.-S. Gal, S. Kang, J. Y. Lee, S.-H. Jin, *J. Mater. Chem. C* **2013**, *1*, 2368-2378.
[30] J. Li, R. Wang, R. Yang, W. Zhou, X. Wang, *J. Mater. Chem. C* **2013**, *1*, 4171-4179.
[31] R. Wang, D. Liu, H. Ren, T. Zhang, X. Wang, J. Li, *J. Mater. Chem.* **2011**, *21*, 15494-15500.
[32] C. Fan, L. Zhu, B. Jiang, Y. Li, F. Zhao, D. Ma, J. Qin, C. Yang, *J. Phys. Chem. C* **2013**, *117*, 19134–19141.
[33] J.-H. Choi, C.-H. Jung, J. Y. Kwon, H.-J. Cho, J. Lee, J.-I. Lee, H.-Y. Chu, D.-H. Hwang, *Synth. Met.* **2009**, *159*, 1517–1521.
[34] M. A. Baldo, S. Lamansky, P. E. Burrows, M. E. Thompson, S. R. Forrest, *Appl. Phys. Lett.* **1999**, *75*, 4–6.
[35] M. G. Colombo, T. C. Brunold, T. Riedener, H. U. Guedel, M. Fortsch, H.-B. Buergi, *Inorg. Chem.* **1994**, *33*, 545–550.
[36] Q. Zhang, B. Li, S. Huang, H. Nomura, H. Tanaka, C. Adachi, *Nat. Photonics* **2014**, *8*, 326–332.
[37] M. Cai, M. Auffray, D. Zhang, Y. Zhang, R. Nagata, Z. Lin, X. Tang, C.-Y. Chan, Y.-T. Lee, T. Huang, X. Song, Y. Tsuchiya, C. Adachi, L. Duan, *Chem. Eng. J.* **2021**, *420*, 127591.
[38] D. Di, A. S. Romanov, L. Yang, J. M. Richter, J. P. H. Rivett, S. Jones, T. H. Thomas, M. Abdi Jalebi, R. H. Friend, M. Linnolahti, M. Bochmann, D. Credgington, *Science* **2017**, *356*, 159–163.
[39] R. Hamze, S. Shi, S. C. Kapper, D. S. Muthiah Ravinson, L. Estergreen, M.-C. Jung, A. C. Tadle, R. Haiges, P. I. Djurovich, J. L. Peltier, R. Jazzar, G. Bertrand, S. E. Bradforth, M. E. Thompson, *J. Am. Chem. Soc.* **2019**, *141*, 8616–8626.
[40] R. Hamze, J. L. Peltier, D. Sylvinson, M. Jung, J. Cardenas, R. Haiges, M. Soleilhavoup, R. Jazzar, P. I. Djurovich, G. Bertrand, M. E. Thompson, *Science* **2019**, *363*, 601–606.
[41] S. Shi, M. C. Jung, C. Coburn, A. Tadle, D. Sylvinson M. R., P. I. Djurovich, S. R. Forrest, M. E. Thompson, *J. Am. Chem. Soc.* **2019**, *141*, 3576–3588.
[42] S. Leuthäußer, D. Schwarz, H. Plenio, *Chem. - A Eur. J.* **2007**, *13*, 7195–7203.
[43] O. Santoro, A. Collado, A. M. Z. Slawin, S. P. Nolan, C. S. J. Cazin, *Chem. Commun.* **2013**, *49*, 10483–10485.
[44] R. Hamze, M. Idris, D. S. Muthiah Ravinson, M. C. Jung, R. Haiges, P. I. Djurovich, M. E. Thompson, *Front. Chem.* **2020**, *8*.
[45] T. Li, D. S. Muthiah Ravinson, R. Haiges, P. I. Djurovich, M. E. Thompson, *J. Am. Chem. Soc.* **2020**, *142*, 6158–6172.
[46] A. S. Romanov, M. Linnolahti, M. Bochmann, *Dalt. Trans.* **2021**, *50*, 17156–17164.
[47] M. Gernert, L. Balles-Wolf, F. Kerner, U. Müller, A. Schmiedel, M. Holzapfel, C. M. Marian, J. Pflaum, C. Lambert, A. Steffen, *J. Am. Chem. Soc.* **2020**, *142*, 8897–8909.

[48] P. K. Samanta, D. Kim, V. Coropceanu, J.-L. Brédas, *J. Am. Chem. Soc.* **2017**, *139*, 4042–4051.
[49] A. J. Lees, *Comments Inorg. Chem.* **1995**, *17*, 319–346.
[50] J. Hossain, R. Akhtar, S. Khan, *Polyhedron* **2021**, *201*, 115151.
[51] I. Piel, M. D. Pawelczyk, K. Hirano, R. Fröhlich, F. Glorius, *European J. Org. Chem.* **2011**, *2011*, 5475–5484.
[52] R. Czerwieniec, J. Yu, H. Yersin, *Inorg. Chem.* **2011**, *50*, 8293–8301.

ACKNOWLEDGEMENTS

The author would like to express his gratitude to the following colleagues for their contribution to the Doctoral Thesis:

- Dr. chem. Kaspars Traskovskis and Dr. chem. Valdis Kokars for supervising the Doctoral Thesis;
- colleagues of the Institute of Applied Chemistry for providing support to the research of the Thesis;
- Dr. chem. Baiba Turovska and Dr. phys. Sergey Belyakov for cyclic voltammetry analysis and X-ray diffraction analyses;
- The team of the Laboratory of Organic Materials of Institute of Solid State Physics of University of Latvia under the leadership of Dr. phys. Aivars Vembris for contribution to various measurements and OLED preparation;
- international partners for their contribution to OLED preparation and DFT calculations;
- Laura Drunka for correcting the manuscript.

Armands Rudušs

The research of the Thesis was financially supported by the Latvian Council of Science grant No. lzp-2019/1-0231 and RTU doctoral grant for doctoral students of the Faculty of Materials Science and Applied Chemistry.

This work has been supported by the European Social Fund within the Project No 8.2.2.0/20/I/008 «*Strengthening of PhD students and academic personnel of Riga Technical University and BA School of Business and Finance in the strategic fields of specialization»* of the Specific Objective 8.2.2 *«To Strengthen Academic Staff of Higher Education Institutions in Strategic Specialization Areas»* of the Operational Programme *«Growth and Employment»*.

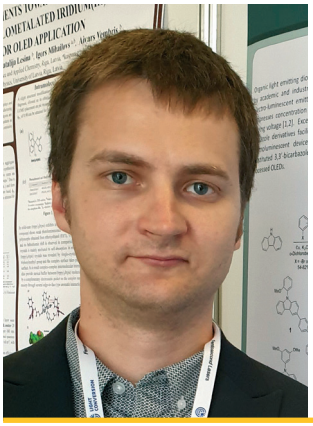

Armands Rudušs was born in 1992 in Limbaži, Latvia. He received his BSc and MSc in Chemical Engineering from Riga Technical University in 2015 and 2017, respectively. A. Rudušs started working at RTU Institute of Applied Chemistry in 2014 as senior laboratory assistant in scientific work. In parallel to work and studies in the field of chemistry A. Rudušs studied at the University of Latvia, obtaining a teacher's qualification (in 2021, second level professional higher education). From 2020 to 2022, he was as chemistry and geography teacher at Ādaži Secondary School. His main scientific interests are related to the synthesis and research of organic materials used in photonics. Currently, Armands Rudušs is a researcher with RTU Institute of Applied Chemistry.